

Effects of topographic structure on salt marsh currents

Raymond Torres¹ and Richard Styles¹

Received 24 March 2006; revised 18 December 2006; accepted 15 February 2007; published 25 May 2007.

[1] The purpose of this study was to assess the spatial and temporal variability in overmarsh and in-channel currents, and to assess that variability in the context of salt marsh topographic structure. We created a high accuracy digital elevation model of a salt marsh island using a real time kinematic Global Positioning System. We measured currents with two velocimeters at the heads of adjacent first order creeks of two separate intertidal creek networks, 30 m apart. We also monitored in-channel currents with one current profiler. All measurements were taken during a 5-day period with spring, mixed tides. Observations reveal that during the high-high tides three current reversals occurred, one during flood, one near peak tide, and another during ebb, as opposed to the usual single reversal near peak tide. These reversals took place in shallow overmarsh flows and in deeper in-channel flows. This current complexity appears to be related to tide elevation and the submergence or emergence of salt marsh topography, and it likely reflects interactions between local topographic forcing and larger scale barotropic pressure gradients. Moreover, when the marsh platform was inundated but under ebb conditions the major components in overmarsh flow patterns between creek heads indicated a regular exchange of water between tidal creek systems. Hence the characterization of overmarsh flows as having flow divides between intertidal creek networks deserves greater scrutiny. Taken together, these observations show that the subtle topography of a salt marsh landscape exerts important control on the temporal and spatial variability on currents at centimeter- to creek network-scales. More research is needed to characterize marsh topography, overmarsh circulation, and their combined effect on material transport and sediment accretion.

Citation: Torres, R., and R. Styles (2007), Effects of topographic structure on salt marsh currents, *J. Geophys. Res.*, 112, F02023, doi:10.1029/2006JF000508.

1. Introduction

[2] Salt marshes are highly productive environments that fringe many temperate midlatitude coastlines. Typically, salt marshes function as intertidal floodplains and their high productivity is maintained by recurring exchanges of matter and energy through intertidal creek networks [Frey and Basan, 1978; Allen, 2000]. These low relief landscapes consequently serve as sediment sinks, and complex hydrodynamic processes facilitate spatially variable patterns of deposition and erosion [e.g., Pestrong, 1965; Reed *et al.*, 1985; French *et al.*, 1995; Leonard, 1997; Christiansen *et al.*, 2000; Temmerman *et al.*, 2005a]. Quantifying overmarsh hydrodynamic processes in these landscapes is important because they strongly influence net sediment accretion, and the distribution of suspended matter, dissolved constituents, seeds and larva. As a result intertidal zone currents exert important controls on ecosystem function, and strategies for salt marsh construction and rehabilitation [e.g., Haltiner and Zedler, 1997].

[3] Salt marshes can be divided into three characteristic zones that are set by elevation; they are the intertidal creeks, the marsh platform, and the upland or levee areas [after Wang and Eisma, 1988]. Creek networks etched into the salt marsh occupy the lower elevations; the higher elevations are associated with levees or with relict terrestrial uplands, and both have limited aerial extent. Intermediate in elevation, the salt marsh platform is most extensive, and has the least relief. Relief between levees (or relict uplands) and creek beds principally varies with tidal range, but field observations show that platform relief is less than 0.3 m [e.g., Eiser and Kjerfve, 1986; Collins *et al.*, 1987; Christiansen *et al.*, 2000], or less than about 0.5 m along macrotidal coasts [French *et al.*, 1995; Davidson-Arnott *et al.*, 2002; Temmerman *et al.*, 2005a, 2005b].

[4] Field studies have shown that salt marsh inundation occurs by apical flow at creek heads and by overbank flow through low points along tidal creeks or larger subtidal channels. For example, French and Stoddart [1992] estimated that ~40% of the overmarsh flows likely originated from creek banks, and recent work by Temmerman *et al.* [2005a] indicates that the value may go up to 60%. This type of inundation from multiple sources is due to salt marsh topographic structure and has been invoked to account for spatial and temporal variability in overmarsh

¹Department of Geological Sciences, Marine Science Program, University of South Carolina, Columbia, South Carolina, USA.

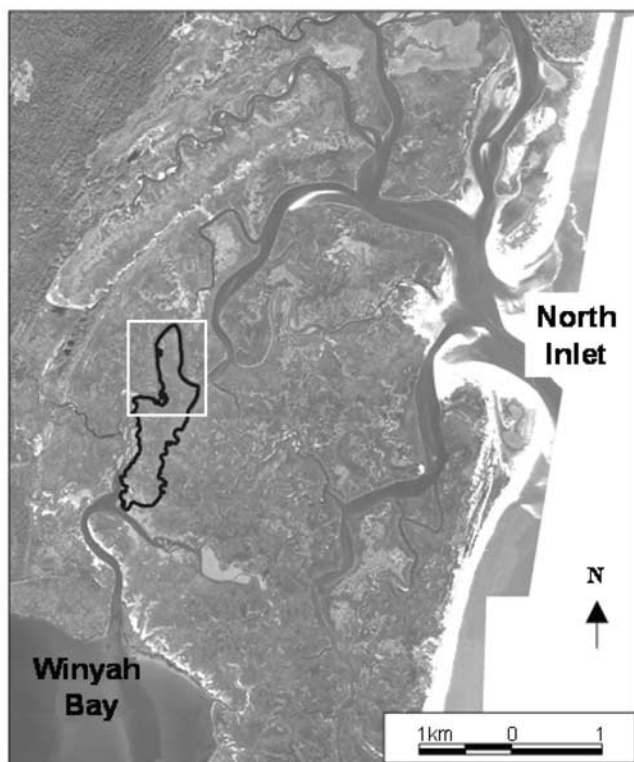


Figure 1. Aerial image of North Inlet estuary with study site, Maddieanna Island, outlined in black with detailed topography of Figure 2 outlined in white. The inlet, North Inlet is at the middle right; Winyah Bay is to the south. Textured dark gray to the upper left is forest, white is sand and the lighter gray is salt marsh. Water-filled channels are smooth dark gray.

currents [e.g., Eiser and Kjerve, 1986; Christiansen *et al.*, 2000; Leonard, 1997; Davidson-Arnott *et al.*, 2002; Temmerman *et al.*, 2005a], and on sediment accumulation [Reed *et al.*, 1985; French and Stoddart, 1992]. On the other hand, numerical simulations by Temmerman *et al.* [2005b] indicate that vegetation effects may induce greater variability in overmarsh currents than does variability in topography. Nevertheless, results from these studies support the assertion of French and Stoddart [1992] that an individual water parcel may follow flow paths that differ significantly between flood and ebb conditions, and it appears that they may facilitate water exchange between individual tidal creek systems. This inference has important implications for watershed area-based conceptualizations and numerical simulations of tidal creek network development and stability [e.g., Rinaldo *et al.*, 1999a and others].

[5] Insight into overmarsh currents, and linking in-channel to overmarsh flow is critical to understanding salt marsh processes because they play a large role in salt marsh morphodynamics [summarized by Allen, 2000; D'Alpaos *et al.*, 2005; Temmerman *et al.*, 2005a]. In particular, Rinaldo *et al.* [1999a] developed a numerical model to characterize high tide hydrodynamic flow divides assumed to exist between distinct intertidal creek systems. This hydrodynamic divide approach is useful because it allows for estimation of intertidal creek watershed area, and this

facilitates analyses of salt marsh dynamics [Rinaldo *et al.*, 1999a, 1999b; Marani *et al.*, 2003; D'Alpaos *et al.*, 2005]. However, the conceptual view that hydrodynamic divides develop and persist between tidal creeks during periods of inundation has not been supported or refuted by field observations, and therefore represents a major assumption in the conceptualization of actual flow conditions.

[6] In this study we mapped the topography of an intertidal landscape, made a set of in-channel and overmarsh current observations, and monitored tide elevation to investigate interactions between topographic structure and salt marsh current complexity. Surprisingly, there are few studies in the peer-reviewed literature that were focused on assessing simultaneous observations of overmarsh and in-channel currents, and how these observations vary with tidal stage. Part of the problem is related to field conditions that limit accessibility, site disturbance resulting from mechanically weak tidal wetland soils, disturbance to fragile vegetation, and the exceptionally large equipment and personnel requirements. Nevertheless, the work presented here provides data and analyses that are likely to improve our understanding of small- and large-scale variability in salt marsh currents, circulation, and sedimentary processes.

[7] The purpose of this study was to measure overmarsh and in-channel currents, and to examine the temporal and spatial patterns in the context of salt marsh topographic structure. Here we propose to: (1) characterize the complexity of overmarsh currents and in-channel currents during spring tide inundations, (2) assess the variability of overmarsh currents between geomorphologically similar locations, and (3) document flow paths between separate but adjacent intertidal creek systems, all in the context of the three-dimensional structure of the landscape.

2. Study Site

[8] The study was conducted in the proximity of 33°19'N, 79°53'W, near Georgetown, South Carolina, USA. The North Inlet marsh-estuary system is a relatively pristine 32 km² bar-built, ebb-dominated, micro tidal (average tide range, ~1.5 m) lagoonal estuary bordered to the south by the broad marsh and mud flat of Winyah Bay, to the east by Holocene barrier islands, and to the west by forested beach ridges (Figure 1). Sinuous subtidal channels (>40 m wide) dissect the expansive low relief intertidal wetlands, and smaller intertidal creeks less than 5 m wide etch the salt marsh platform. For example, in an 8.7-km² area of intertidal marsh there are 725 of these small scale tidal creek networks; total creek length is 114 km, giving an average drainage density of 13.1 km/km² [Novakowski *et al.*, 2004]. During low tide these smaller creeks may be dry or have negligible downstream flow, whereas the larger subtidal channels retain about 1–3 m water depth during neap tide lows.

[9] The western edge of the salt marsh is on topographically higher relict side slopes of beach ridges, but seaward, away from the terrestrial environment, the maximum relief results from levees formed on the banks of larger tidal channels. Differences in marsh elevation distinguish high marsh from low marsh, and they are reflected in the distribution of vegetation. Seaward, the vegetation transitions from maritime forest to *Juncus roemerianus* to *Salicornia*

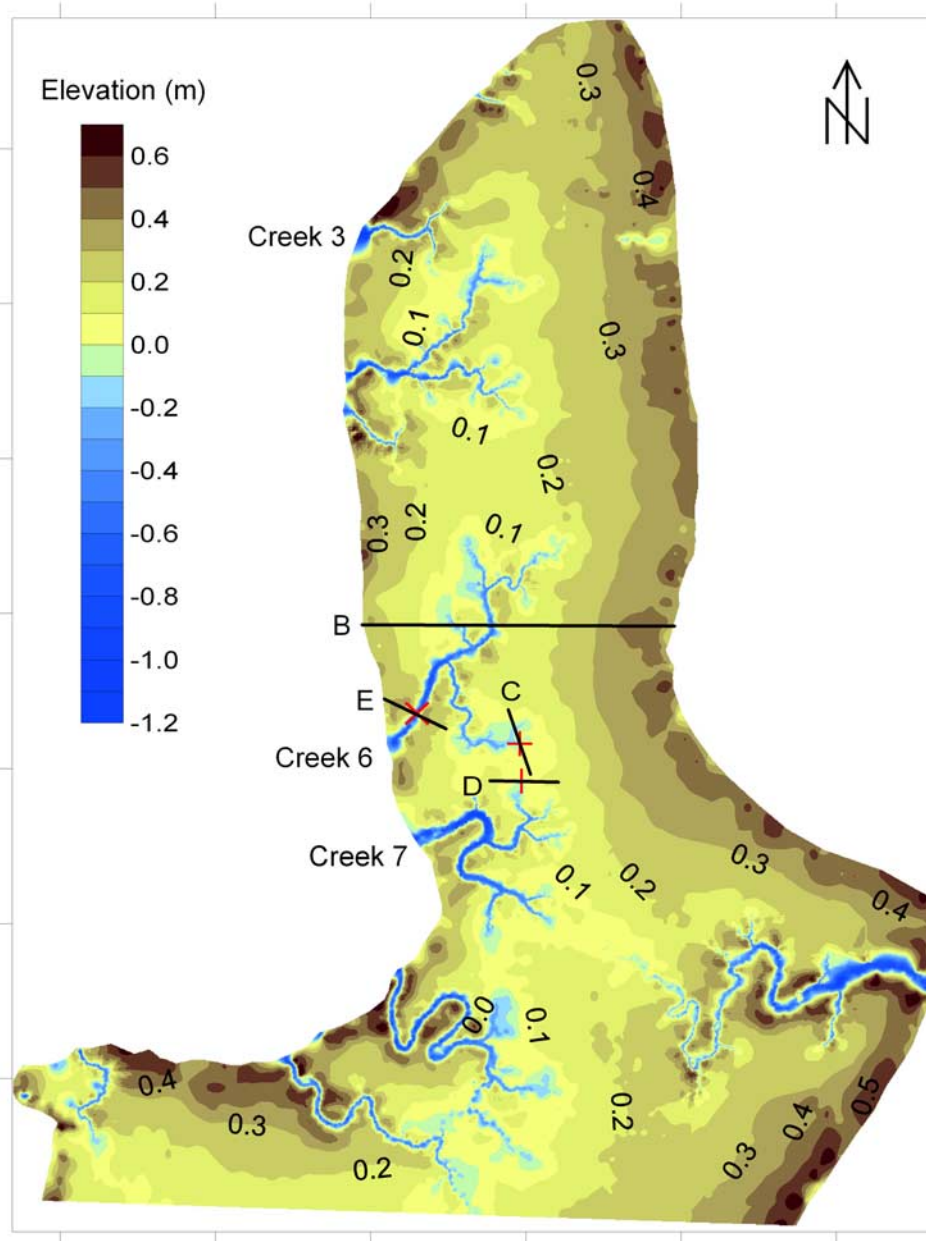


Figure 2. Color relief map of the north part of Maddieanna Island; color shades correspond to 0.1-m intervals. The island is bound to the north by a >40 m wide subtidal channel. Creeks 6 and 7 are the monitoring sites, the red positive symbols represent the ADV positions; the x mark represent the ADCP position. Solid black lines depict locations where topographic transects were made and shown in Figure 3. Each tick on the axes corresponds to 100 m. Note the higher levees on the east relative to the west side.

virginica to short *Spartina alterniflora* to tall *Spartina alterniflora* in the low marsh. Typically, the channel banks have tall *S. alterniflora*, and short *S. alterniflora* is on the levees. Stem heights and density vary seasonally, but in summer most stem heights on the levees are within 0.2–0.4 m, and on the lower marsh 0.8–1.1 m [Morris and Haskin, 1990]. The regularly inundated channels and pans are fine-grained and unvegetated. Eastern oyster (*Crassostrea virginica*) reefs are common along the marsh edge, and they may cover the entire wetted perimeter of smaller intertidal creek mouths, becoming patchy and less common upstream.

[10] The study area is on the northern part of a salt marsh island, Maddieanna Island (Figures 1 and 2). The island is not directly linked to any terrestrial upland area and therefore it is fully within the intertidal zone, approximately 1 km from the forest-marsh edge. The northern part of the island is bound by a U-shaped turn in the ~55 m wide subtidal channel (Figure 1). This major channel is directly connected to an inlet (North Inlet) approximately 7 km along channel to the east, and it is open to Winyah Bay, approximately 3 km to the south. Traynum and Styles [2007] contend that the subtidal channel bounding the island on the west is a mixing zone for these two water

sources. The entire island may be submerged during spring tides, but during neap tides the marsh platform remains largely subaerial. Water surface slopes in the subtidal zone at a site 2 km north were estimated at 1.2×10^{-4} m/m [Eiser and Kjerve, 1986].

[11] In the northern part of the island where our study was conducted there are 11 discrete intertidal tidal creek systems with channel length ranging from tens to hundreds of meters. Our study was focused on two of the larger third order creek systems, creeks 6 and 7 (Figure 2). Creek 6 is a dendritic system and has a total stream length of 478 m, and creek distance from mouth to the creek head nearest creek 6 is 155 m, or 73 m in a straight line. Upstream of the creek head was an approximately 10 m long, 0.1 m vegetated depression trending 075° . Creek 7 is meandering and has a total stream length of 322 m and distance to creek head nearest creek 6 is 125 m, or 70 m in straight line; upstream there was a 4 m long shallow vegetated depression trending 030° . Both creeks had oysters on the bed and banks, and oyster shells on the bed extended for about 40 m upstream becoming patchy with distance from the creek mouth.

[12] We identified the peak daily tides of the diurnal cycle for the 2004 tidal record from the US NOAA Oyster Landing tide gauge (PID DD1345) and ranked them to show that neap tide peaks were greater than 0.19 m and spring peaks were up to 1.51 m, while the median peak tide was 0.85 m. Maximum tidal elevation observed during our study was 0.98 m. Maximum elevation in the study area is 0.67 m but the bulk of the salt marsh is much lower (Figure 2). Therefore during this study the salt marsh platform was fully inundated at high tide, and at low tide the marsh platform and levees were subaerial.

3. Methods

[13] A real time kinematic Global Positioning System (GPS) total station with Trimble 5700 dual frequency receivers was used to create a digital elevation model (DEM) of Maddieanna Island at North Inlet, South Carolina. The base receiver was positioned over "D Tidal", a NGS order 1 benchmark (PID DD1355). Additional geodetic control was provided by two order 1 benchmarks that were installed for this study and are now part of the NGS national database (PID AJ5765 and AJ5767). The combined ground control provided 0.02 and 0.02 m accuracy in the horizontal and vertical, respectively. Distance from the base receiver to the study area was variable but at most 3 km, with a clear line of sight. GPS data were acquired over 2 years. The marsh platform position data were acquired at 4–10 m spacing, depending on local topographic variations. The creek edges data have approximately 0.5 m spacing to fully identify creek banks, and the creek bed and lower bank GPS points were spaced at 0.5–2 m. The levee areas have approximately 2 m spacing (Figure 2). Special care was taken to place the GPS receiver pole on the sedimentary surface. Given the potential for operator error under the less than ideal field conditions at times (for example, sinking into mud, insect bites, heat) we estimate that the vertical accuracy for the DEM used is 0.04 m, and the horizontal accuracy is 0.04 m. All elevations in this study were referenced to NAVD 88. The DEM data presented in Figure 2 represents 31,000 points, the northern subset of a total of 77,000 points taken to characterize the

entire island (Figure 1). The data were interpolated onto a 0.25-m grid using an inverse distance weighting procedure in Surfer, length and areas were evaluated in ARC GIS, and vector and scalar data were analyzed using Matlab.

[14] In order to visualize overmarsh tidal circulation, and to assess the occurrence of hydrodynamic flow divides between two discrete intertidal creek networks during high tide we installed two current meters at two adjacent but separate first order creek heads (Figure 2). Two autonomous Sontek acoustic Doppler velocimeters (ADV) and pressure gauges were placed at adjacent creek heads between creeks 6 and 7 (Figure 2); hence, these instruments were installed to monitor currents at geomorphologically similar locations, channel heads. The ADVs sampled a roughly cubic centimeter volume at a rate of 10 Hz and they were programmed to record data for a 10-min burst every 20 min; the 10-min data were averaged to give mean vertical, north and east current components every 20 min. All measurements reported here coincide with a mixed spring tides (diurnal high and low tides with different elevations) from 2 to 7 June 2004.

[15] The ADVs were installed horizontally with the long axis of the instrument oriented along topographic contour and normal to expected flow paths. This configuration allowed us to detect currents for a longer part of the submergence interval. Also, with this orientation the current meter is less likely to be affected by turbulence in flows passing the sensor body where the electronic components are housed. We compensated for the orientation of the resulting side-looking velocity measurements. The data from the ADVs provided three components of flow although our analyses focus on the north and east directions. The creek 6 ADV monitored flows at an elevation of 0.00 (approximately 0.1 m above the mud surface), and the creek 7 ADV monitored flows at 0.01 m (approximately 0.08 m above the mud surface). The ADV sites were intermittently subaerial with each tidal cycle, and the locations coincide with the approximately 1.5 m wide transition zone linking bare mud to densely vegetated marsh platform. From digital photographs we estimated the *S. alterniflora* stem density around the instruments at less than 10 stems/m².

[16] The ADVs were 30.1 m apart with the creek 6 site on a bearing 357° from the creek 7 site (Figure 2). The area separating these instruments is unchanneled and *S. alterniflora*-vegetated marsh platform with plant top elevations at approximately 0.8–1.1 m. In conducting this study we walked over the marsh surface one time going from the creek 6 to creek 7 ADV sites. In the process we created a 0.4-m wide preferential flow path (bearing 357°) through the bent and broken grass, and it had not recovered in the time frame of the study. Nevertheless, our observations show that flow directions did not necessarily coincide with the nearly north-south pathway.

[17] We also monitored in-channel currents for the same time interval at a location 36.7 m upstream of the mouth of creek 6 (Figure 2). Here we used an upward looking 2 MHz Nortek Aquadopp acoustic Doppler current profiler (ADCP). The ADCP position is shown in Figure 2; it is in a relatively straight reach of the creek with an approximately U-shaped cross section profile. The instrument was downstream of all major tributaries and sensors were at

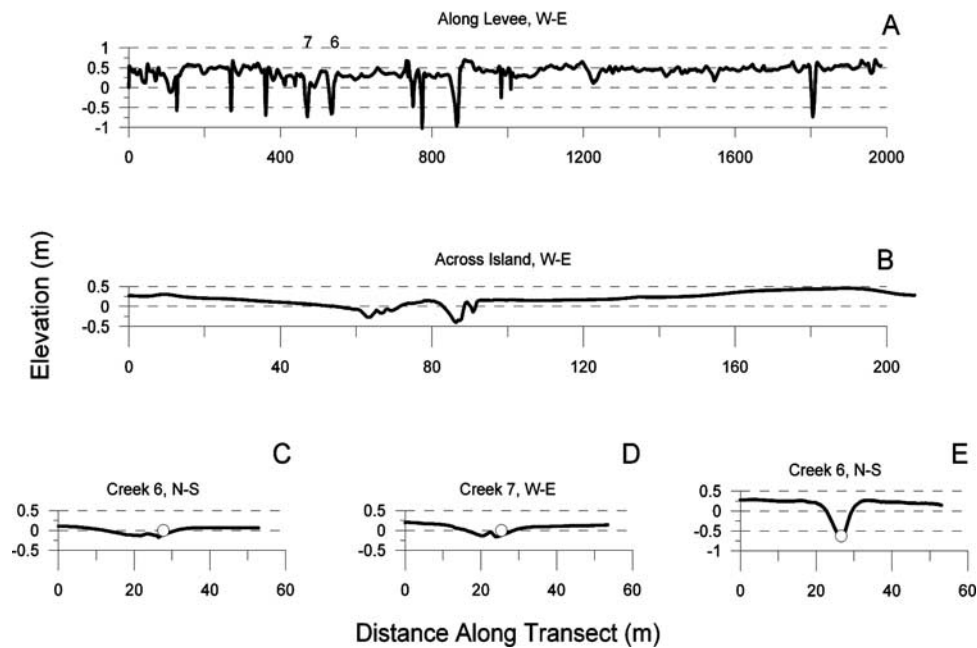


Figure 3. Cross-sections of topography, vertical exaggeration on Figure 3a is 100:1, and 10:1 on Figures 3b–3e. Figure 3a is a clockwise profile along the outer edge of the northern part of the island shown in Figure 2. The profile runs along the levee crest, and through the levee breaks and creek mouths. Note the relatively uniform elevation along the western edge, from 1240–1680 m. Figure 3b is a profile across the island through upper creek 6. Note the subtle trough structure. Figures 3c and 3d are profiles from the ADV current meter sites. Note the outer edges of the transect in creek 7 are higher than for creek 6. Figure 3e shows the transect across the ADCP site of creek 6. The total area of flow up to the creek banks is 4.6 m². Open circles are centered on ADV sites in Figures 3c and 3d, and the ADCP site in Figure 3e.

0.1 m above the creek bed, at an elevation of -0.63 m. The profiler sampled at a rate of 1 Hz. The 1 Hz data were averaged internally every 5 min to produce a mean current at each bin. The lowest of the 20 bins with 0.1-m spacing was located at 0.1 m above the transducer head, which placed it approximately 0.2 m above the creek bed or at -0.53 m. The profiler also contained an absolute pressure transducer to measure water depth and all water surface elevations reported here are referenced to this pressure transducer, following atmospheric corrections. Based on our observations the low high (LH) tide inundated all but the levees, while during the high high (HH) tide intervals the entire area was submerged, consistent with spring tide levels. Net channel velocity was estimated as a depth averaged value that only included nonzero bins. Hereafter, we refer to “upstream” and “downstream” flows by using “upstream” to describe in-channel flow directed toward the channel head, and “downstream” flows as in-channel flow away from the creek head, toward the creek mouth.

[18] The North Inlet-Winyah Bay NERR maintains a tide and meteorological station approximately 4 km north of the study site. We corrected the absolute pressure sensor data giving water depth with the local barometric readings. The weather station also acquires 1-min wind velocity observations and saves them as 15-min averages. We used these wind velocity measurements to compare with the current vector data to examine the effects of wind on overmarsh currents. The wind speed data were recorded as meter per second and the wind directions were recorded as the

azimuth from which the wind blew. These directional data were converted to north and east vector components.

4. Results

4.1. Salt Marsh Topography

[19] Maximum salt marsh elevation was 0.67 m with a minimum of -1.17 m, both near the mouth of creek 3 (Figure 2); total relief therefore was 1.84 m, but relief between the platform and levees was approximately 0.6 m. The relief on the marsh platform itself, however, was limited to about 0.3 m. The 0.0 m contour line in Figure 2 approximately identifies the bare mud-vegetation transition, with bare mud at the lower elevations. Tidal creeks dissect a peripheral levee at the creek mouths and they have dendritic or meandering patterns, and all creeks terminate near the middle of the island at about 0.0 m elevation (Figure 2). The levee is well developed albeit discontinuous with the eastern levees being higher, wider, and more continuous than on the west (Figure 2). Assuming that the levee base is at 0.3 m, and creeks terminate at 0.0 m, the marsh platform is bound by the 0.0 and 0.3 m contours. In this case the platform occupies 81% and the levees occupy 14% of the area in Figure 2. Also, note that creek banks may be at a higher or lower elevation than the creek head.

[20] Figure 3a depicts a topographic profile along the levee that goes clockwise, around the outer edge of the island (Figure 2). The profile runs along the levee crest, and through the levee breaks and creek mouths. Overall, the

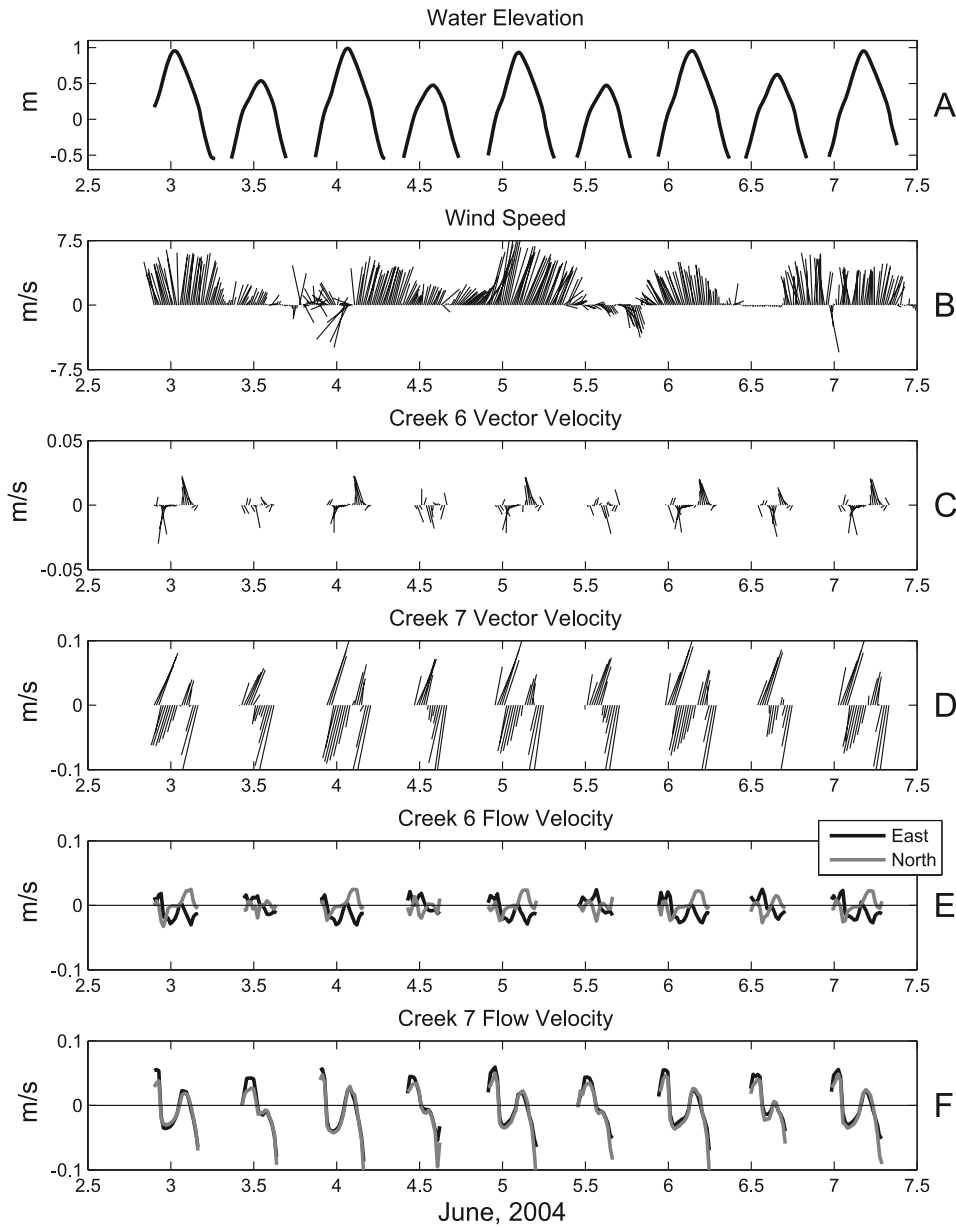


Figure 4. Time series of tide elevation, wind and current vectors, and current speed. Figure 4a is tide elevation measured with the ADCP in creek 6. Note the mixed tides and the maximum low-high tide near day 6.5. Figure 4b is a feathered plot of wind vectors. Figures 4c and 4d are current vector plots at creeks 6 and 7, respectively. Note the diurnal pattern of three and one current reversals during high-high and low high tide, respectively, with the low-high tide near day 6.5 being the exception. Figures 4e and 4f are the north and east current velocity components. Note the three-flow reversal in high-high creek 7 data, and in the north component of the creek 6 data.

profile shows a highly irregular western edge relative to the east, and it shows that the creek mouths do not “bottom out” at the same elevation. Moreover, in the vicinity of creeks 6 and 7 there is an overall depression in the island perimeter that is up to 0.25 m lower than the average levee tops to the east. Meanwhile, the eastern edge is higher and the levee crest elevations are relatively uniform.

[21] A topographic profile across the island is shown in Figure 3b (profile location shown on Figure 2). Overall, the levees give rise to a subtle asymmetrical depression with a nearly flat interior. The levee elevation to the east reached

0.48 m while on the west it was 0.32 m. The slopes from the levees to the platform are comparable, 0.005 m/m on the west (at 20–40 m on Figure 3b) and 0.007 m/m on the east (at 150–170 m). Figure 3b also shows an approximately trapezoidal profile through an upper reach of creek 6 and some smaller tributaries (see Figure 2). Figures 3c and 3d highlight the topographic profiles at the ADV sites with the instruments at 24.4 and 27.7 m, respectively. The profiles had very subtle relief, as expected, but an overlay will show that the sides of the creek 7 site were 0.010–0.15 m higher. Therefore creek 7 had a higher cross-section area of flow

Table 1. Summary of Tide Stage and Time (Relative to Peak Tide) of Current Reversals^a

HH	First Reversal		Second Reversal		Third Reversal	
	Elevation	Time	Elevation	Time	Elevation	Time
<i>Creek 6</i>						
N	0.27–0.39	–2.6–2.1	0.82–0.92	0.5–0.8	0.24–0.35	2.9–3.2
E	0.47–0.54	–2.0–1.6	0.84–0.86	0.5–0.8	0.74–0.76	1.0–1.3
<i>Creek 7</i>						
N	0.42–0.48	–2.3–1.8	0.84–0.88	0.6–0.8	0.42–0.47	2.3–2.4
E	0.42–0.48	–2.3–1.8	0.84–0.88	0.6–0.8	0.42–0.47	2.3–2.4
Velocity Profiles	0.50–0.54	–1.8–1.5	0.82–0.88	0.8–1.0	0.60–0.65	1.5–2.0
Depth Average Velocity Profiles	0.48–0.55	–2.0–1.5	0.80–0.88	0.5–0.9	0.58–0.65	1.5–2.0
Creek 7 slope break	0.43–0.53	–0.7–0.3				
<i>LH, day 6.5</i>						
Creek 7	0.48	–1.1	0.59	0.2	0.44	1.0
Velocity Profile	0.53	–0.6	0.56	0.7	0.61	0.3

^aElevations are in meters and times are in hours. N and E refer to north and east current components, respectively. HH and LH refer to high high and low high tides, respectively.

compared to creek 6 due to its apparently higher level of “channelization”. Finally, the creek profile for the ADCP site depicts a U-shaped cross section (but V-shaped in the figure due to vertical exaggeration). The total area of flow was 4.6 m² (Figure 3e).

[22] During the study the HH tides ranged from 0.92–0.98 m and the LH tides were between 0.48–0.61 m; the low tide elevations were below the pressure sensor elevation of –0.63 m (Figure 4a). Wind speeds and directions were variable, but predominantly from south to north (Figure 4b). Maximum speed was 7.6 m/s and there were roughly two half-day intervals of calm conditions at day 3.5 and 6.5. The higher wind speeds and overall prevailing direction was toward 015°–040°. The lower wind speeds were more variable and toward 315°–135°; there were negligible occurrences of slight winds toward 135°–315°. On the basis of the recurring daily pattern, the variability in wind speed and direction seemed not to affect variability in overmarsh currents (Figures 4b, 4c, and 4d).

4.2. Flow Characteristics at Creek 7

[23] Blanks in the current velocity time series (Figure 4) correspond to intervals when the ADVs were subaerial. During marsh inundation the maximum velocity at creek 7 was 0.14 m/s although most observations were less than 0.10 m/s, and currents were typically to the northeast or southwest. During HH tides three well-defined flow reversals occurred, for example, conditions where both flow components transitioned between positive or negative values (Figures 4d and 4f). During the LH tides there was a single reversal near peak tide, although the LH inundation of day 6.5 also had three reversals. Ordinarily, one might expect a single flow reversal associated with peak tide, thus the HH and single LH reversals are scrutinized below.

[24] For each HH tide, one flow reversal occurred during flood, one occurred shortly after peak tide, and the third was during ebb tide. In Table 1 we present the observed range of times and elevations for these reversals. The middle, or second reversal came about within 0.6–0.8 hr after peak tide, at tide elevations of 0.84–0.88 m. The first reversals

were observed at 0.42–0.48 m, and during ebb the third reversals were at 0.42–0.47 m. In summary, at the head of creek 7, flow on the flood tide was initially upstream, when the tide reached 0.42–0.48 m flow direction changed to downstream. Shortly after peak tide, with the tide stage at 0.84–0.88 m the overmarsh currents transitioned to upstream, but as the tide declined to 0.42 to 0.48-m current direction switched to downstream.

[25] The peak LH tides from days 3–6 were 0.51, 0.48, 0.49, and 0.61 m, respectively (Figure 4a), and the corresponding currents show a single flow reversal (Figure 4d). However, the time series of current components show a break in slope in the middle of each LH time series indicating a declining rate of change (Figure 4f). This break in slope came about at 0.3–0.7 hr preceding peak tide, with a corresponding tide level of 0.43–0.53 m. This elevation range is comparable to tide levels where reversals were clearly detected on the HH tides (Table 1). On the other hand, the LH response of day 6.5 is distinct from the LH signal of preceding days (Figures 4d and 4f). For example, on this tide three flow reversals developed, as with the HH tides, albeit of much shorter duration and lower magnitude. Moreover, the first reversal on the flood stage happened at 0.48 m, shortly before peak tide. The second and third LH reversals arose after peak tide at 0.59 and 0.44 m, respectively. These values are comparable to the HH reversal elevations, but the middle reversal developed at much lower tide stage. Thus, the day 6.5 signal helps assign a lower limit to the tide elevation at which reversals occur, 0.61 m, slightly higher than the levee. Moreover, the 0.45–0.50 m tide elevation range has emerged as a threshold for flood and ebb flow reversals to occur that appear not to be related to overall changes in the barotropic pressure gradient.

4.3. Flow Characteristics at Creek 6

[26] At creek 6 the current data were markedly different and we initially thought the instrument failed (Figures 4c and 4e). However, on-site checks and post-experiment laboratory tests indicated that the data were representative of actual field conditions. Thus, there is large variability in current direction and especially magnitude between geo-

morphologically similar observation points. The maximum current speed was 0.04 m/s with most readings less than 0.02 m/s. The HH tides produced faster currents with regular patterns of southerly flow on the flood tide, to negligible flow, to a stronger northerly current after peak tide. The LH tides were much more variable although the LH response on day 6.5 again resembled the HH response (Figure 4c). Also, the variations in peak velocity were out of phase between flow components, unlike that observed at creek 7. Also, the large temporal variations in net current direction principally results from east-west flow component variability (Figures 4c and 4e).

[27] In order to assess the reversal patterns in creek 6 currents and the corresponding elevations it was useful to consider each flow component separately (Figure 4e). With the north component there were clear differences between HH and LH responses. The HH response principally had one cycle of southern flows that transitioned to northern flows. Between the peak north and south velocities was a roughly 2-hr interval of near 0.0 m/s flow to the south. The flow reversals that we focus on here are those that occurred prior to the peak southern flow, the one at the end of the 0.0 m/s flow interval, just after peak northern flow (Table 1). The first reversals occurred at 0.27–0.39 m and within 2.6 to 2.1 hr preceding peak tide. The second reversal at 0.82–0.92 m arose shortly after peak tide. The third reversals were in an elevation range comparable to the first, 0.25–0.35 m, about 3 hr after peak tide. Meanwhile, the east component was distinct from the north component, and HH and LH responses differed as well (Figure 4e). For example, HH currents had longer duration flows to the west and a single cycle of east-west fluctuations, similar to the creek 7 response. Other similarities to creek 7 exist. For example, the first reversals were at 0.47–0.54 m, and the second were at 0.84–0.86. On the other hand, the third reversal happened at 0.75 m.

[28] The approximately north-south positioning of ADV sites and the relatively short distance separating them (30 m) allows one to visually compare the current velocity vectors in (Figures 4c and 4d) to assess flow convergence or divergence. The faster ebb currents were to the northwest at creek 6 and they coincided with northeastern currents at creek 7. Therefore on the ebb tide there was a recurring northerly flow from creek 7 to creek 6. On the other hand, the weaker flood currents were to the south at creek 6, and these coincided with currents to the north emanating from creek 7. Hence, on the flood tide there appears to be weakly convergent flow. Overall, the flow convergence indicates that there are flow divides on the flood tide, but on the ebb tide current directions indicate a net transport of water from creek 7 to creek 6. In other words, there were flow divides between creeks on the flood tide but not on ebb.

[29] Together these data indicate that overmarsh currents were highly variable in space and time, and at creek heads currents may experience three reversals. The second or middle reversal was likely related to the change in barotropic pressure gradient, but the first and third not necessarily so. These two reversals came about with peak tides greater than ~ 0.61 m, and typically developed in the tidal elevation range of 0.45–0.55 m. Moreover, the current reversals observed with the ADVs for shallow overmarsh

flows also occurred with deeper in-channel flows as detected with the ADCP in creek 6.

4.4. Flow Characteristics in the Tidal Creek

[30] The June 5 ADCP time series is presented as representative of all time series in this study. These data show that in-channel currents mimicked the flow reversals described above, and these flow reversals were detected throughout the entire water column (Figure 5). For example, with the onset of the HH flood (Figure 5a) the upstream currents were between 0.0–0.15 m/s (-4.4 to -3.3 hr). Later (-3.3 hr), currents in the entire profile increased to approximately 0.45 m/s within 0.17 hr. This rapid and large change corresponded to a tidal elevation range of 0.0–0.1 m, and the increase was likely associated with apical flows filling local low-lying areas (Figure 2). As tide stage increased the velocities increased and peaked at about 0.55 m/s (-2.7 to -2.1 hr) at an elevation range of 0.2–0.3 m, inundating much of the lower marsh and filling the island basin. At a stage height of 0.40–0.50 m (-1.8 hr), there was an abrupt transition in velocity showing a decline and flow reversal, all within 0.17 hr. At 0.40–0.50 m most of the marsh was inundated, and completely inundated at 0.7 m (-1.5 hr), although the taller grass stalks were above this level.

[31] After a peak tide of 0.93 m the downstream flow continued until a reversal with weak upstream flow occurred at +0.5 hr, and during complete marsh inundation (Figure 5a). As the tide ebbed to 0.60–0.70 m topography and vegetation emerged, and the upstream flow intensified to 0.2 m/s (1.2 hr). Later, from 0.60 to 0.50 m (+1.8 to +2.2 hr) surface flows appeared to be moving upstream while at depth the flow was downstream. Later the reversal was complete and thereafter water flowed downstream. Downstream velocities rapidly increased at 0.40–0.50 m and peaked at ~ 0.6 m/s (+3.5 hr), and then declined to 0.10 m/s at +3.8 hr or -0.1 m. As with the ADV data, the in-channel ADCP data show identical flow reversals, with downstream flow during the flood interval, and upstream flow during the ebb interval (Table 1).

[32] On the LH flood tide (Figure 5b) the upstream velocities gradually increased from less than 0.05 to 0.50 m/s, reaching the higher value at a tide stage of 0.1–0.2 m (-4 to -2 hr). Peak flood velocities were 0.5–0.6 m/s (-1.5 hr) at 0.2–0.3 m, followed by a sharp decline to ~ 0.1 m/s when the tide stage was 0.40–0.50 m (-0.8 hr). During the slack tide, from -0.8 to +0.5 hr, the current profile had both upstream and downstream flow, with no particular organization. From +0.5 to +0.7 hr the upper profile had upstream flow and the lower was downstream, all at 0.5–0.6 m. Thereafter, the downstream velocity intensified, reaching a peak of ~ 0.5 m/s at 0.00–0.10 m (+1.9 hr). At -0.1 –0.0 m there was an abrupt transition from high to low velocity (+2.2 hr), continuing to weaken as the tide ebbed. In summary, the ADCP and the ADV data give a consistent story with corresponding flow reversals on the HH, and none on the LH with reversals occurring at roughly the same elevations (Table 1). Also, the HH speeds were generally higher, and the LH water profile had upstream and downstream flow.

[33] All in-channel ADCP data are summarized in Figure 6 as depth averaged velocity plotted against water surface

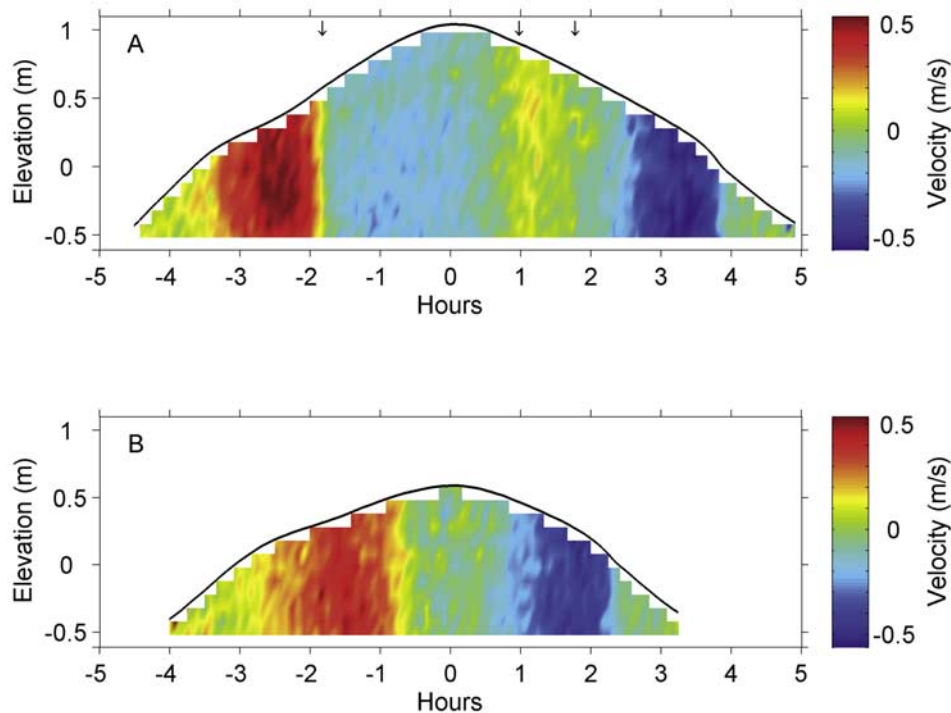


Figure 5. Time series of velocity profiles from creek 6 on June 5. Figure 5a corresponds to high-high tide and Figure 5b is for the low-high tide. Reds indicate upstream flow and the blues indicate downstream flow. Note the three sharp flow reversals that occur on the flood and ebb tide stages of the high-high tide, and the single reversal on the low-high tide. Arrows show flow reversals summarized in Table 1 and the black line is tide elevation.

elevation. Here we are able to refine estimates of elevation because we use ± 0.01 -m resolution pressure data as opposed to 0.1-m bin elevation data above. Typically, the HH velocities were greater than the LHs, but the most striking aspect of this plot is the clear “figure-8” shape, consistent with the flow reversals discussed above. Asymmetry in both lobes of the figure-8 results from sharper peaks in upstream flow, and from differences in the elevation of peak velocity during flood and ebb conditions. For example, upstream flows peaked at 0.25–0.35 m and at ~ 0.80 m, while downstream flows peaked at 0.10–0.20 m and at ~ 0.85 m. The overlapping HH and LH data highlight a consistent response in all tidal signals.

[34] Typically, on the flood tide, the upstream velocities were highly variable between elevations of -0.5 – 0.0 m while flow was confined to the channel. Above 0.0 m the velocity increased at a uniform rate with stage height up to approximately 0.3 m, but this was followed by a steady decline up to 0.5 m at which point the current reversed. In fact, the fastest decline occurred between 0.4 – 0.5 m where just three readings per cycle (0.25 hr) cover the corresponding decrease in velocity from 0.25 to -0.05 m/s. The crossover elevation in the figure-8 is at approximately 0.55 m, coincident with the submergence of all but the highest elevations (Figure 2). The corresponding crossover velocity was about -0.07 m/s. From there the downstream velocity increased slightly up to water level of 0.75 m. Peak tide was at about 0.95 m and it was followed by a downstream velocity decrease, reaching 0.0 m/s at 0.87 m; the subsequent upstream current maximum was 0.1 m/s at

0.80 m. Thereafter, the velocity declined and reversed at 0.65 m, and the downstream velocity increased steadily down to 0.15 m.

[35] With the falling tide below 0.15 m the velocity decreased at a steady rate down to -0.1 m with a rapid change in stage height from 0.0 to -0.1 m. Below that flow was again confined to the channel. These observations highlight the flow reversals described above and they illustrate the asymmetry in the in-channel velocity response to stage height. Moreover, the ebb dominant velocity asymmetry characteristic of the estuary [Eiser and Kjerve, 1986] is not present in this small scale tidal creek, although there was ebb dominance in the duration of ebb as suggested by the enclosed areas on either side of the 0.0 m/s line (Figure 6). This asymmetry may be related to water having to flow uphill as it inundates the marsh platform, but on the ebb the free surface and topographic gradients were directed toward the middle of the island, and toward the low area at the mouths of creeks 6 and 7 (Figures 2, 3a, and 3b).

5. Discussion

[36] One of the main outcomes of this work is related to the observations and conceptual model used to explain how salt marsh topography affects centimeter- to creek network-scale spatial and temporal variability in overmarsh currents. During salt marsh inundation the overmarsh current patterns exhibit sudden changes that are related to the overtopping or submergence of salt marsh topography. When the salt marsh topography is partly emergent current patterns appear to be

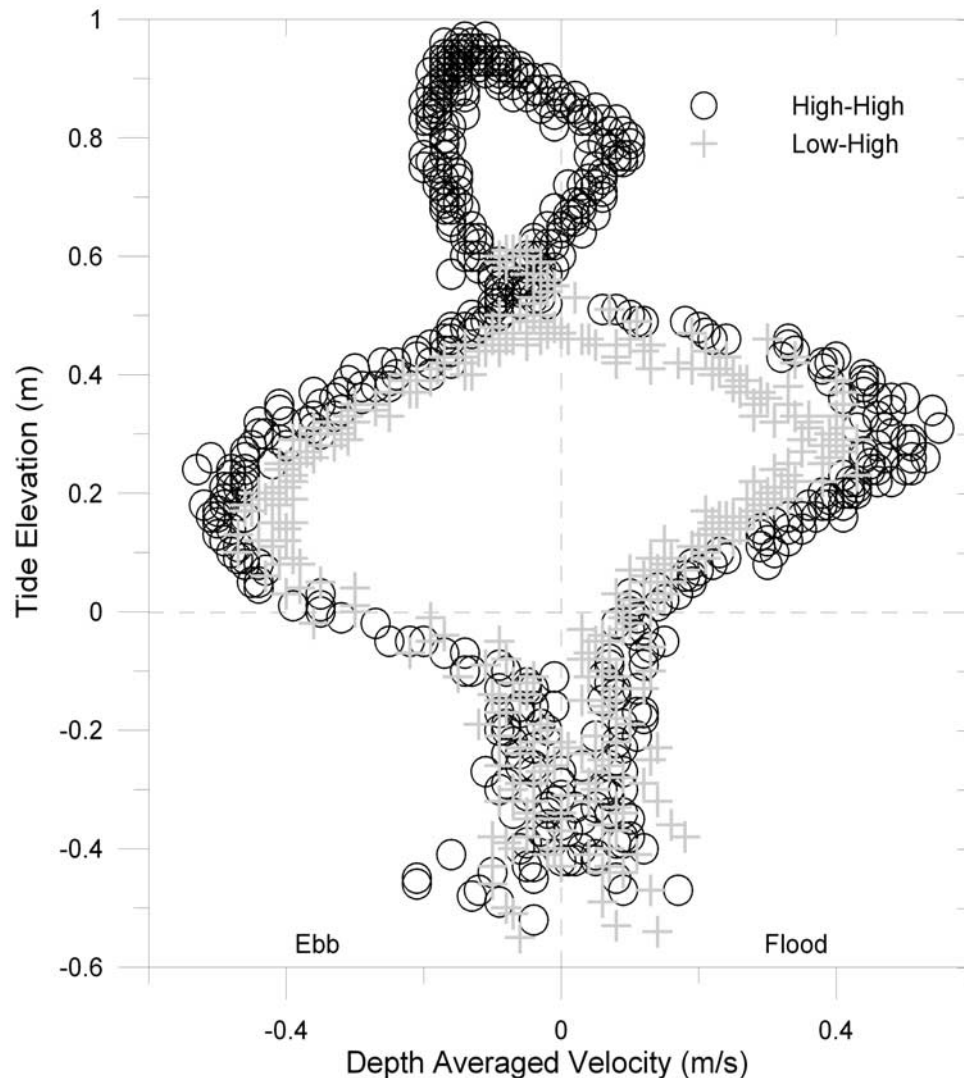


Figure 6. Velocity-stage height relationship from the profiler depth averaged velocity data in creek 6. The empty circle symbols represent all high-high conditions and the cross symbols represent all low-high tides. Note the “figure-8” shape and the three instances where the trends in the data cross the 0.0 m/s line, indicating flow reversals.

controlled by flow routing through the tidal creeks. When the marsh is fully submerged current patterns suddenly change and are controlled by larger-scale pressure gradients. This flow complexity appears to lead to the exchange of water between distinct tidal creek basins and calls into question the idea of applying “watershed basin area” concepts to intertidal zone geomorphic modeling of tidal landscape evolution [e.g., *Rinaldo et al.*, 1999a]. These general findings are discussed in more detail below.

5.1. Spatial Variability in Flow

[37] Despite positioning current meters only 30 m apart, at the same elevation and in geomorphologically similar locations, there were large differences in current magnitude and direction, and in temporal variability between creek 6 and creek 7 sites. These differences may have resulted from variations in cross-sectional areas of flow between sites. For example, the creek 7 site was in a narrower, better defined channel segment than creek 6 (Figures 3c and 3d). More-

over, the creek 7 site has a 0.15-m ridge to the west (Figure 2) and this likely helped confine flows. Consequently, it appears that very subtle variations in topography may account for the observed spatial variability in overmarsh velocity measurements. Alternatively, effects of the prevailing creek structure may have played a role in the variability as well (Figure 2). For example, the creek 6 site is in a mostly east-west trending channel reach, whereas the creek 7 site is in a mostly north-south trending reach. Thus, in order to account for variations in the north-south component of creek 6 data it appears that a larger overmarsh pressure gradient promotes south to north flow.

[38] Creeks 6 and 7 are “mutually exclusive” [after *Allen*, 2000] intertidal creek systems meaning that their respective channelized segments do not intersect (Figure 2). Hence creeks 6 and 7 are separated by a swath of slightly higher, vegetated and unchanneled marsh platform. Field observations show that current directions between the facing outer edges of these creek networks had convergent flow on the

flood tide (Figures 4c and 4d). On ebb tides greater than 0.3 m, when the platform separating the creeks was inundated, the currents indicated south to north flow. This south to north flow may have been aided by southerly winds (Figure 4b), but not necessarily so as demonstrated by wind and current patterns of day 5–5.5. Together, these observations support the idea that water may be exchanged between separate tidal creek networks during high tide inundation. Consequently, these results call into question the utility of geomorphic concepts related to flow divides, “watershed boundary”, “watershed divide”, and “watershed area” in intertidal creek network and landscape analyses [e.g., *Fagherazzi et al.*, 1999; *Novakowski et al.*, 2004, and others], including those defined by hydrodynamic modeling [*Rinaldo et al.*, 1999a, 1999b, and others]. Questions arise because flow routing and hydrodynamics and resulting sedimentary or erosional processes in salt marshes may not necessarily be dictated by watershed area or flow divide concepts at all. Of course, the watershed divide concept is valid on the flood tide, but when the platform is overtopped, the times presumed to coincide with maximum work [*Rinaldo et al.*, 1999b], this may not be the case. Nevertheless, more work is needed to support or refute the development of flow divides between intertidal creek networks.

5.2. Flow Reversals

[39] In the Bay of Fundy salt marshes, *Davidson-Arnott et al.* [2002] report short-lived flow reversals that took place within 0.5 hr on either side of peak tide. These flow reversals, however, were of a relatively low magnitude (<0.01 m/s) and were a short-lived (<0.2 hr) component of the total overmarsh flow field. Likewise, *Christiansen* [1998] reports current data with similar flow reversals near peak tide but they are not discussed, and much of the effect may have been filtered out (pg. 44). Moreover, *French and Stoddart* [1992] report flood tide data showing salt marsh water surface slopes declining to 0.0 m/m and then increasing to a peak value, and then declining again with a reversal at peak tide; this sequence was repeated on ebb. Hence the data indicate that during the flood and ebb stages there is an emerging flow reversal. Although an actual slope (or flow) reversal did not occur on flood or ebb we contend that this response may be an indication of the start of a flow reversal, comparable to the weakly developed reversal associated with the maximum LH response of day 6.5 (Figure 4d). Thus, flow reversals during ebb and during flood appear to be regular features of in-channel and overmarsh currents in micro to macrotidal landscapes at various longitudes but they have not been well characterized or explained, and their effects on material cycling and morphodynamics are not known. The dearth of field studies focused on flow complexity may be related to the general perception that the occurrence of flow reversals is limited to changes in barotropic pressure gradient or to the occurrence of peak tide, and anything in addition to the major reversal at peak tide is noise.

[40] To relate these reversals to topographic structure we summarize in Table 1 the elevations and times relative to peak tide at which reversals occurred. The ADV data reveal aspects of the flow reversals, and nascent reversals that are common to each instance, including the short-lived LH

reversal of day 6.5. For example, on the LH flood tides most of the breaks in slope in the velocity time series occur at about 0.45–0.50 m (Figure 4f). During the HH flood tides the first current reversals at creek 7 and in the north component of creek 6 were between 0.45–0.55 m. This first reversal is followed by the expected barotropic gradient driven reversal near peak tide at 0.80–0.90 m. Later, as the tide ebbed, a third flow reversal came about but the tide elevations were more variable (Table 1). The creek 6 east component reversed at 0.75 m, while the north component reversed at about 0.30 m; both the creek 7 components reversed at ~0.45. On the other hand, the ADCP depth averaged data indicate that the first reversals occurred at 0.48–0.55 m, and shortly after peak tide at 0.80–0.88 m, and again at 0.58–0.65 m. Thus most of the ADV and ADCP data are in approximate agreement on the elevation of the first and second reversals, at 0.50 ± 0.05 m and 0.85 ± 0.05 m, respectively, but not on the third.

[41] Here we endeavor to explain the occurrence of flow reversals in the context of salt marsh topographic structure; elevations reported below represent a range of ± 0.05 m. Assuming that Figure 6 represents the bulk average hydrodynamic response, current observations reveal that at the onset of the flood tide the relatively weak flows coincide with the filling of the tidal creeks. At approximately 0.0-m tidal stage, the generally higher creek bank elevations near the mouth of creek 6 facilitate apical flows at creek heads and thereby limit overbank flows to upstream of the ADCP (Figure 2). These flows lead to inundation of the broad marsh platform, and as the tide continues to rise the in-channel flows accelerate. Once the platform is covered, at ~0.3 m, the basin mostly fills up (upward). Hence the lateral spreading of water ends, and the rate of upstream water delivery and corresponding in-channel velocity must decline. The in-channel velocity continues to decline until most of the island is submerged at 0.5–0.6 m (Figure 2), including the levees along the east edge of the island. Consequently, at 0.5–0.6 m a direct hydraulic connection between the subtidal creek and intertidal creeks develop, and through this connection the advancing tidal wave may propagate over the marsh surface. This hydraulic connection produces the first current reversal, transitioning from upstream to downstream flow. As the tide continues to rise to a tide stage of 0.7 m the island is completely submerged. From 0.7 m to peak tide the velocity is relatively constant.

[42] After peak tide, at the start of ebb, the downstream flow weakens but persists. This is well known for shallow frictionally dominated estuaries with significant intertidal storage, where a delay between slack water (current reversal) and high water results from nonlinear processes [e.g., *Friedrichs and Aubrey*, 1988]. This leads to an asymmetry between flood/ebb maximum current speed and tidal stage, described below. As the stage lowers the downstream flows weaken and at ~0.85 m upstream flow develops. We interpret this second reversal to be associated with a reversal in barotropic pressure gradient that changes flow direction toward North Inlet (Figure 1). As the tide level continues to decline the upstream flow peaks and reverts to the downstream direction, the third reversal. The commencement of the third reversal corresponds to different elevations, but the bulk average current response from the ADCP data indicates a reversal at 0.60 m. At this elevation most of the

marsh is still submerged, therefore we speculate that the reversals at this tide stage are associated with the combined effects of vegetation drag and form drag (emergent topography).

[43] In contrast, the ADV data at creek 7 consistently record the third reversal as taking place at 0.45 m. This elevation corresponds to a large scale and mostly complete hydraulic disconnect of the free surface due to the now subaerial levees on the east side (Figures 2 and 3). Therefore water flowing toward the inlet can no longer traverse the salt marsh island to the observations points but must now remain in the subtidal channel and flow around the island perimeter. Moreover, due to the emergent boundary condition the remnant water on the marsh must flow from east to west as the tide declines. Meanwhile, the creek 6 currents are not as readily characterized and we do not fully understand their variability. Nevertheless, the third reversal for the east component occurs at 0.75 m, but note that the interval between the second and third reversals is less than 0.5 hr (Figure 4e). Thus, we speculate that this short reversal interval is an indication of some transient condition indicating the “setting up” of the bulk average and site specific reversals, similar to the water surface slope observations of *French and Stoddart* [1992]. Thus, there is evidence showing that salt marsh topographic structure may control the timing of current reversals and overmarsh flow complexity in general.

[44] On the other hand, numerical simulation results from *Temmerman et al.* [2005a, 2005b] indicate that elevation and salt marsh structure have a subordinate effect on overmarsh and in-channel current complexity relative to salt marsh vegetation. In the present study vegetation seems not to exert the same influence on flow complexity. This inference is supported by the facts that the reversals during flood occur over a narrow elevation range that exactly coincides with the levee tops (Figure 3), and the second reversals occur near peak tide. Consequently, vegetation drag likely does not affect the first or second current reversals. Nevertheless, the high variability in water levels at which the third reversal occurs may result from the combined effects of vegetation drag and topographic forcing (for example, creek 6 observations). For example, *Temmerman et al.* [2005a, 2005b] report that when the water level is below the canopy the contrast between the hydraulically rough vegetated platform and the smoother channels causes water to be preferentially transported through the channel. However, when the water level is above the canopy, the difference in roughness is diminished so that larger scale sheetflow will develop, likely controlled by the larger scale pressure gradient. This variability in roughness with stage height may account for some of the reversals that do not coincide well with the higher levee elevations (Table 1).

5.3. Conceptual Model

[45] Figures 7a–7j summarize our conceptual model describing inundation of Maddieanna Island and they help explain the observed flow conditions in Figures 4, 5, and 6. Figure 7 contains a series of panels showing a highly idealized cross-section profile of the northern part of the island through, for example, creek 6. Therefore the creek mouth is on the left of each panel and the creek bed is shown as a concave up dashed line. Arrows of various

lengths depict flow magnitude and direction (upstream or downstream), and the horizontal bold lines indicate the water surface stage. Figures 7a–7e represent the rising tide with the free water surface sloping to the left (for example, pressure gradient from North Inlet to the mouth of creek 6). The ebb tide water surface in Figures 7f–7j slopes to the right (for example, pressure gradient from creek mouth to inlet), as indicated at the top of each column.

[46] In Figure 7a the tide is rising and it produces weak upstream flow as the channel fills. In Figure 7b the water level reaches the creek banks and the upstream flow is still weak. As the water level continues to rise the delivery of water to the marsh increases rapidly (Figure 7c) until the various creek networks become hydraulically connected. At that point the marsh island basin continues to fill from the creek systems, much like a bathtub. Hence the water level continues to rise until the levees are overtopped (Figure 7d). At that point the in-channel flow directions are no longer dictated by filling or draining from the mouth. Instead, the currents are controlled by the overall slope of the advancing tidal wave. Hence when the stage height exceeds the levee tops the in-channel flow transitions from upstream flow controlled by water entering the creek through its mouth a flow system controlled by the larger scale sloping water surface. In this sense, topography damps the immediate effects of the tidal wave on currents and exerts a first order control on in-channel currents. As the water level continues to rise the downstream current increases slightly (Figure 7e).

[47] The flow reversal from Figures 7e–7f occurs because the tidal wave has passed the island and the water surface slope has changed direction, and flow is now upstream. In Figure 7g when the stage height drops below the levee tops the boundary effects on flow cause the in-channel flow to again reverse direction and flow downstream to the creek mouth. As the water level declines further more water is forced to leave the system through the creek mouth and a higher downstream current results (Figure 7h). As the marsh continues to drain the various creek networks become hydraulically distinct, and in-channel current velocity declines (Figure 7i), and it continues to decline as the channels themselves drain (Figure 7f).

[48] Now the question is: Under what conditions is topographic structure likely to induce the type of flow complexity observed at our field site? To address this question we propose that intertidal landscapes be distinguished between those areas with a direct connection to a terrestrial boundary, and those without one, for example, salt marsh areas separated from the mainland by large subtidal channels. Intertidal marsh platform areas with terrestrial boundaries are less likely to be inundated from the upstream side of the marsh, and therefore are most frequently inundated from the mouths of creeks or at low points along the banks. Conversely, in areas where the intertidal zone has no direct connection to terrestrial uplands or where the tidal and subtidal channels are highly sinuous the marsh platform may be inundated by overbank flows, especially on marsh islands or peninsulas. However, the issue of hydraulic connectivity between individual salt marsh basins (for example, flow from creek 6 to creek 7) is likely independent of terrestrial-intertidal boundaries.

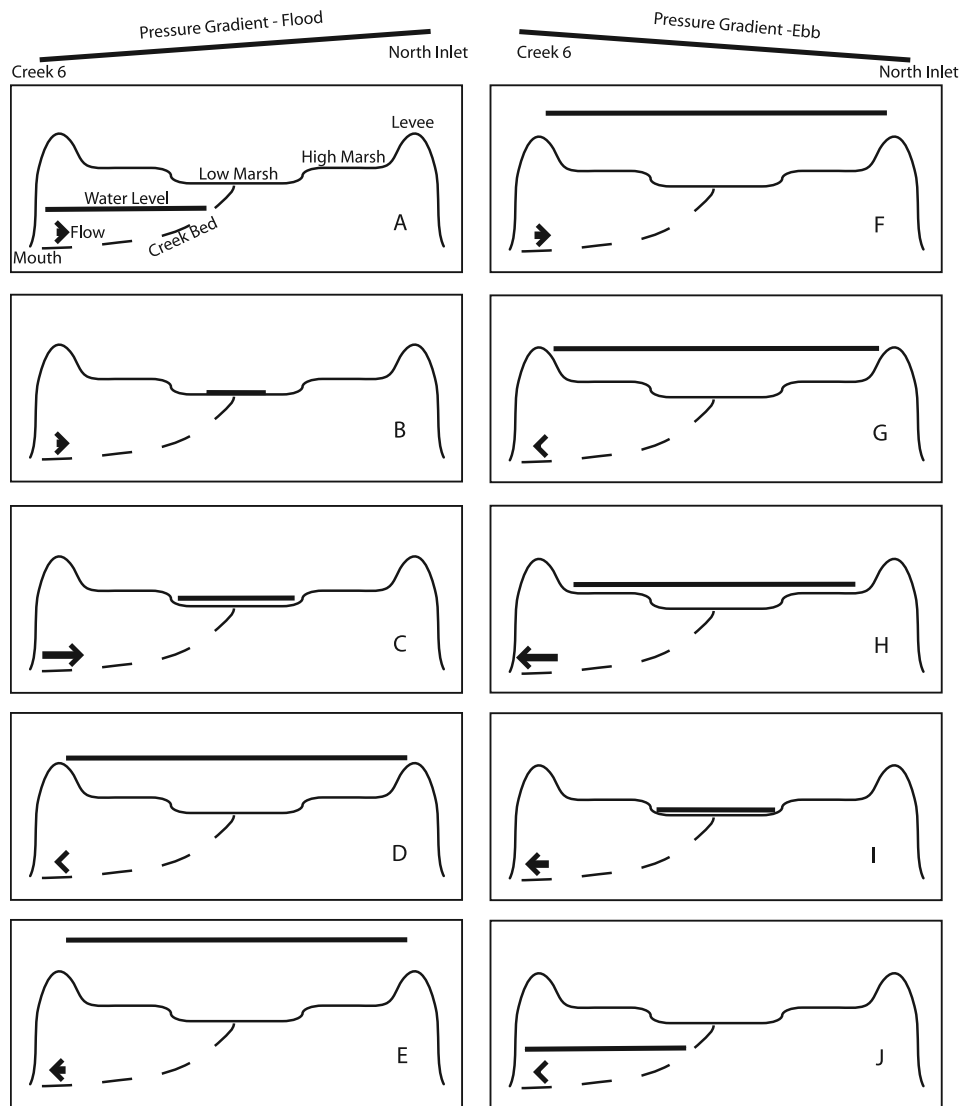


Figure 7. Panels showing a highly idealized topographic cross section of the island. Arrows depict in-channel velocity changes with tide stage (heavy horizontal black line) as a time series with Figures 7a–7e for the flood tide, and Figures 7f–7j corresponding to the ebb tide. Note the larger scale free water surface slope at the top of each column corresponding to flood (from North Inlet) and ebb (toward North Inlet, Figure 1), directions, respectively. Flow reversals occur between Figures 7c–7d, 7e–7f, and 7f–7g.

[49] We propose that the observed flow reversals are related to the combination of creek orientation and direction of the pressure gradient. For example, at our site, on a rising tide the pressure gradient dictates that water flow from east to west. The position of the mouth and orientation of creek 6, however, dictate that the in-channel currents run from west to east. When the levees are overtopped the flow is then from east to west. Conversely, we speculate that the observed in-channel flow reversals will not occur in tidal creeks with mouths open on the east side of the island (Figure 2) because the creek mouth is open in the direction of the incoming or outgoing tidal wave. Taken together these observations and conceptual model show that the three-dimensional structure of the salt marsh exerts boundary effects on the free surface such that the very subtle salt marsh topography appears to control, in part, the temporal

and spatial variability of velocity at centimeter-scale point measurements of overmarsh currents, and of creek network-scale in-channel currents. We speculate that there is a role played by vegetations that may alter the elevations at which the observed flow reversal occurs [e.g., *Temmerman et al.*, 2005a, 2005b] but this remains to be shown. Clearly, more research is needed to understand the controls on, and the effects of temporally and spatially variable overmarsh currents, overmarsh circulation, and the interactions between overmarsh currents and marsh morphodynamics.

6. Conclusions

[50] Point measurements of overmarsh currents from two locations reveal high variability in space and time despite being only 30 m apart, at the same elevation and in geomorphologically similar locations. Also, during the

higher tides the ebbing flow vectors at both sites had predominantly south to north flows, thereby indicating an exchange of water between discrete tidal creek networks. These observations suggest that the use of “watershed” boundary concepts in tidal creek network morphodynamics analyses require further evaluation and field verification.

[51] The point measurements and in-channel water column velocity profile data show that all of the higher high tides had three flow reversals, one during flood, one near peak tide and another during ebb. The first reversal took place as the rising tide reached the levee tops, thus providing a direct hydraulic connection between the subtidal creek system and the salt marsh interior. The second reversal is likely associated with a reversal in the barotropic pressure gradient since it occurs at or near peak tide. The third reversal occurs with the emergence of the salt marsh topography and the resulting disconnect in the marsh platform-channel hydraulic connection.

[52] Together, these observations suggest that the complexity of flows over salt marsh landscapes can be explained, in part, by the interactions between salt marsh three-dimensional structure and the free water surface elevation. Moreover, the data show that the three-dimensional structure affects current speed and direction at spatial scales ranging from centimeter-scale point measurements to bulk averaged flows in tidal creek networks. Moreover, over-marsh flow properties indicate that a distinction be made between salt marsh areas with a direct terrestrial connection and those without. Those areas without a direct connection are likely to be in the middle of the intertidal landscape and therefore susceptible to inundation from many different locations. Salt marshes with a direct terrestrial connection have an upstream flow boundary and are likely to fill and drain from fewer points. Overall, these observations and analyses reveal that the very subtle salt marsh relief and position in the broader salt marsh landscape are important facets that affect hydrodynamic processes. Therefore salt marsh circulation should not be oversimplified in studies designed to quantify marsh accretion, marsh morphodynamics, or ecosystem processes.

[53] **Acknowledgments.** This research was supported by the following grants: NSF 9985345, EPA STAR R828677, and ONR N00014-02-1-0972. Kevin White assisted with instrument deployment, and Joe Jurisa helped with data analyses. The South Carolina Geodetic Survey installed benchmarks and worked with Dr. Xiaobo Zhou and Juana Montane to acquire the DEM data. The North-Inlet Winyah Bay NERR provided logistical support, and tide and weather station data. We thank Dr. Stijn Temmerman and an anonymous reviewer for their comments that helped improve manuscript depth and clarity.

References

- Allen, J. R. L. (2000), Morphodynamics of Holocene salt marshes: A review sketch from the Atlantic and Southern North Sea coasts of Europe, *Quat. Sci. Rev.*, *19*, 1155–1231.
- Christiansen, T. (1998), Sediment deposition on a tidal salt marsh, Ph.D. thesis, University of Virginia, 135 p., August.
- Christiansen, T., P. L. Wiberg, and T. G. Milligan (2000), Flow and sediment transport on a tidal salt marsh surface, *Estuar. Coast. Shelf Sci.*, *50*, 315–331.
- Collins, L. M., J. N. Collins, and L. B. Leopold (1987), Geomorphic processes of an estuarine marsh: Preliminary results and hypotheses, in *International Geomorphology, Part 1*, edited by Gardiner, V., p. 1049–1065, John Wiley, Hoboken, N. J.
- Davidson-Arnott, R. G. D., D. vanProosdij, J. Ollerhead, and L. Shostak (2002), Hydrodynamics and sedimentation in salt marshes: Examples from a macrotidal marsh, Bay of Fundy, *Geomorphology*, *48*, 209–231.
- D’Alpaos, A., S. Lanzoni, M. Marani, S. Fagherazzi, and A. Rinaldo (2005), Tidal network ontogeny: Channel initiation and early development, *J. Geophys. Res.*, *110*, F02001, doi:10.1029/2004JF000182.
- Eiser, W. C., and B. Kjerfve (1986), Marsh topography and hypsometric characteristics of a South Carolina salt marsh basin, *Estuar. Coast. Mar. Sci.*, *23*, 331–345.
- Fagherazzi, S., A. Bortoluzzi, W. E. Dietrich, A. Adami, S. Lanzoni, M. Marani, and A. Rinaldo (1999), Tidal networks: I. Automatic network extraction and preliminary scaling features from Digital Elevation Maps, *Water Resour. Res.*, *35*(12), 3891–3904.
- French, J. R., and D. R. Stoddart (1992), Hydrodynamics of salt marsh creek systems: Implications for marsh morphological development and material exchange, *Earth Surf. Processes Landf.*, *17*, 235–252.
- French, J. R., T. Spencer, A. L. Murray, and N. S. Arnold (1995), Geostatistical analysis of sediment deposition in two small tidal wetlands, Norfolk, UK, *J. Coast. Res.*, *11*, 308–321.
- Frey, R. W., and P. B. Basan (1978), Coastal salt marshes, in *Coastal Sedimentary Environments*, edited by R. A. Davis, pp. 225–301, Springer, New York.
- Friedrichs, C. T., and D. G. Aubrey (1988), Non-linear tidal distortion in shallow well-mixed estuaries: A synthesis, *Estuar. Coast. Shelf Sci.*, *27*, 521–545.
- Haltiner, J., and J. B. Zedler (1997), Influence of physical processes on the design, functioning and evolution of restored tidal wetlands in California (USA), *Wetlands Ecol. Manag.*, *4*(2), 73–92.
- Leonard, L. (1997), Controls of sediment transport and deposition in an incised mainland marsh basin, southeastern North Carolina, *Wetlands*, *17*, 263–274.
- Marani, M., E. Belluco, A. D’Alpaos, A. Defina, S. Lanzoni, and A. Rinaldo (2003), On the drainage density of tidal networks, *Water Resour. Res.*, *39*(2), 1040, doi:10.1029/2001WR001051.
- Morris, J. T., and B. Haskin (1990), A 5-year record of aerial primary production and stand characteristics of *Spartina alterniflora*, *Ecology*, *71*(6), 2209–2217.
- Novakowski, K. I., R. Torres, L. R. Gardner, and G. Voulgaris (2004), Geomorphology of intertidal creek networks, *Water Resour. Res.*, *40*(5), W05401, doi:10.1029/2003WR002722.
- Pestrong, R. (1965), The development of drainage patterns on tidal marshes, Ph.D. dissertation, Stanford University, 135 p., April.
- Reed, D. J., D. R. Stoddart, and T. P. Bayless-Smith (1985), Tidal flows and sediment budgets for a salt marsh system, Essex, England, *Vegetation*, *62*, 375–380.
- Rinaldo, A., S. Fagherazzi, S. Lanzoni, M. Marani, and W. E. Dietrich (1999a), Watershed delineation and comparative network morphology, *Water Resour. Res.*, *35*(12), 3905–3917.
- Rinaldo, A., S. Fagherazzi, S. Lanzoni, M. Marani, and W. E. Dietrich (1999b), Landscape forming discharges and studies in empirical geomorphic relationships, *Water Resour. Res.*, *35*(12), 3919–3929.
- Temmerman, S., T. J. Bouma, G. Govers, Z. Wang, M. B. De Vries, and P. M. J. Herman (2005a), Impact of vegetation on flow routing and sedimentation patterns: Three-dimensional modeling for a tidal marsh, *J. Geophys. Res.*, *110*(F4), F04019, doi:10.1029/2005JF000301.
- Temmerman, S., T. J. Bouma, G. Govers, and Z. B. D. Lauwaet (2005b), Flow paths of water and sediment in a tidal marsh: Relations with marsh developmental stage and tidal inundation height, *Estuaries*, *28*(3), 338–352.
- Traynum, S., and R. Styles (2007), Flow, stress and sediment resuspension in a shallow tidal channel, *Estuaries and Coasts*, *30*, 1–8.
- Wang, B. C., and D. Eisma (1988), Mudflat deposition along the Wenzhou coastal plain in southern Zhenjiang, China, in *Tide Influenced Sedimentary Environments and Facies*, edited by deBoer, P. L., pp. 265–274, Springer, New York.

R. Styles and R. Torres, Department of Geological Sciences, Marine Science Program, University of South Carolina, Columbia, SC 29208, USA. (torres@geol.sc.edu)